FirstPage

Pure Spin Current Injection in Hydrogenated Graphene Structures

Reinaldo Zapata-Peña[1], Bernardo S. Mendoza[1], Anatoli I. Shkrebtii[2]

[1]*Centro de Investigaciones en Óptica, León, Guanajuato 37150, México and*

[2]*University of Ontario, Institute of Technology, Oshawa, ON, L1H 7L7, Canada*

(Dated: May 3, 2017)

Lorem ipsum dolor sit amet, consectetuer adipiscing elit. Etiam lobortis facilisis sem. Nullam nec mi et neque pharetra sollicitudin. Praesent imperdiet mi nec ante. Donec ullamcorper, felis non sodales commodo, lectus velit ultrices augue, a dignissim nibh lectus placerat pede. Vivamus nunc nunc, molestie ut, ultricies vel, semper in, velit. Ut porttitor. Praesent in sapien. Lorem ipsum dolor sit amet, consectetuer adipiscing elit. Duis fringilla tristique neque. Sed interdum libero ut metus. Pellentesque placerat. Nam rutrum augue a leo. Morbi sed elit sit amet ante lobortis sollicitudin. Praesent blandit blandit mauris. Praesent lectus tellus, aliquet aliquam, luctus a, egestas a, turpis. Mauris lacinia lorem sit amet ipsum. Nunc quis urna dictum turpis accumsan semper.

I. INTRODUCTION

Lorem ipsum dolor sit amet, consectetuer adipiscing elit. Etiam lobortis facilisis sem. Nullam nec mi et neque pharetra sollicitudin. Praesent imperdiet mi nec ante. Donec ullamcorper, felis non sodales commodo, lectus velit ultrices augue, a dignissim nibh lectus placerat pede. Vivamus nunc nunc, molestie ut, ultricies vel, semper in, velit. Ut porttitor. Praesent in sapien. Lorem ipsum dolor sit amet, consectetuer adipiscing elit. Duis fringilla tristique neque. Sed interdum libero ut metus. Pellentesque placerat. Nam rutrum augue a leo. Morbi sed elit sit amet ante lobortis sollicitudin. Praesent blandit blandit mauris. Praesent lectus tellus, aliquet aliquam, luctus a, egestas a, turpis. Mauris lacinia lorem sit amet ipsum. Nunc quis urna dictum turpis accumsan semper. Lorem ipsum dolor sit amet, consectetuer adipiscing elit. Etiam lobortis facilisis sem. Nullam nec mi et neque pharetra sollicitudin. Praesent imperdiet mi nec ante. Donec ullamcorper, felis non sodales commodo, lectus velit ultrices augue, a dignissim nibh lectus placerat pede. Vivamus nunc nunc, molestie ut, ultricies vel, semper in, velit. Ut porttitor. Praesent in sapien. Lorem ipsum dolor sit amet, consectetuer adipiscing elit. Duis fringilla tristique neque. Sed interdum libero ut metus. Pellentesque placerat. Nam rutrum augue a leo.

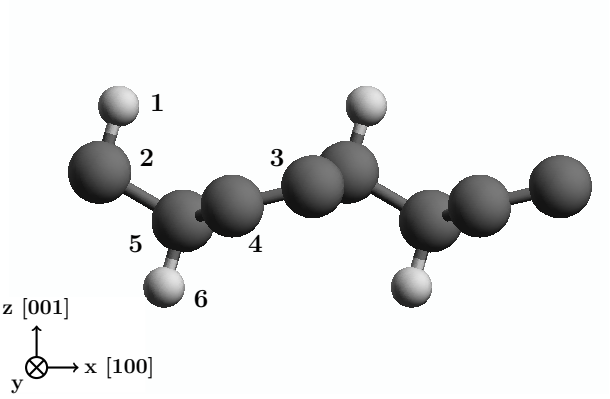

(a) *xz* plane view

fig:alt-struc-xz

(b) *xy* plane view

fig:alt-struc-xy

FIG. 1. Alt structure

fig:alt-struc

Morbi sed elit sit amet ante lobortis sollicitudin. Praesent blandit blandit mauris. Praesent lec-

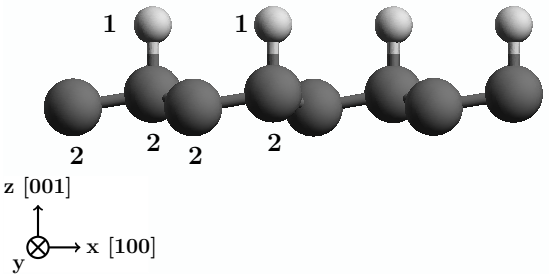

(a) xz plane view fig:up-struc-xz

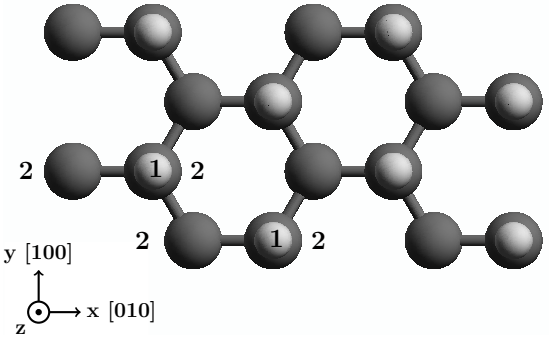

(b) xy plane view fig:up-struc-xy

FIG. 2. Up structure fig:up-struc

tus tellus, aliquet aliquam, luctus a, egestas a, turpis. Mauris lacinia lorem sit amet ipsum. Nunc quis urna dictum turpis accumsan semper. Lorem ipsum dolor sit amet, consectetuer adipiscing elit. Etiam lobortis facilisis sem. Nullam nec mi et neque pharetra sollicitudin. Praesent imperdiet mi nec ante. Donec ullamcorper, felis non sodales commodo, lectus velit ultrices augue, a dignissim nibh lectus placerat pede. Vivamus nunc nunc, molestie ut, ultricies vel, semper in, velit. Ut porttitor. Praesent in sapien. Lorem ipsum dolor sit amet, consectetuer adipiscing elit. Duis fringilla tristique neque. Sed interdum libero ut metus. Pellentesque placerat. Nam rutrum augue a leo. Morbi sed elit sit amet ante lobortis sollicitudin. Praesent blandit blandit mauris. Praesent lectus tellus, aliquet aliquam, luctus a, egestas a, turpis. Mauris lacinia lorem sit amet ipsum. Nunc quis urna dictum turpis accumsan semper.

Lorem ipsum dolor sit amet, consectetuer adipiscing elit. Etiam lobortis facilisis sem. Nullam nec mi et neque pharetra sollicitudin. Praesent imperdiet mi nec ante. Donec ullamcorper, felis non sodales commodo, lectus velit ultrices augue, a dignissim nibh lectus placerat pede. Vivamus nunc nunc, molestie ut, ultricies vel, semper in, velit. Ut porttitor. Praesent in sapien. Lorem ipsum dolor sit amet, consectetuer adipiscing elit. Duis fringilla tristique neque. Sed interdum libero ut metus. Pellentesque placerat. Nam rutrum augue a leo. Morbi sed elit sit amet ante lobortis sollicitudin. Praesent blandit blandit mauris. Praesent lectus tellus, aliquet aliquam, luctus a, egestas a, turpis. Mauris lacinia lorem sit amet ipsum. Nunc quis urna dictum turpis accumsan semper.

II. THEORY

sec:theory

A. Pure spin velocity

sec:theory-pure_spin_current

The spin density injection current $\dot{K}^{\mathrm{ab}}$ with speed along direction a and spin polarization along b is defined as

$$\dot{K} = \mu^{\mathrm{abcd}}(\omega) E^{\mathrm{c}}(\omega) E^{\mathrm{d}*}(\omega) \quad (1)$$ eq:dotk

where

$$\mu^{\mathrm{abcd}}(\omega) = \frac{\pi e^2}{\hbar^2} \int \frac{d^3K}{8\pi^3} \sum_{vcc'}{}' \mathrm{Re}\left[K^{\mathrm{ab}}_{cc'}(r^{\mathrm{c}}_{vc'} r^{\mathrm{d}}_{cv} + r^{\mathrm{d}}_{vc'} r^{\mathrm{c}}_{cv})\right] \delta(\omega - \omega_{cv}) \quad (2)$$ eq:mu

is the corresponding spin density injection current pseudotensor. The $'$ in the sum means that c and c' are quasi degenerate states and the sum only covers these states.

Now we define the spin velocity, $\mathcal{V}^{\rm ab}$ as the speed at which the spin polarized in the b direction moves along the a direction when a normal incident beam reaches the xy plane with a polarization angle α. Then,

$$\mathcal{V}^{\rm ab}(\omega) = \frac{2}{\hbar}\frac{\mu^{\rm abxx}(\omega)E^2(\omega)\cos^2(\alpha) + \mu^{\rm abyy}(\omega)E^2(\omega)\sin^2(\alpha) + 2\mu^{\rm abxy}(\omega)E^2(\omega)\cos(\alpha)\sin(\alpha)}{\xi^{\rm xx}(\omega)E^2(\omega)\cos^2(\alpha) + \xi^{\rm yy}(\omega)E^2(\omega)\sin^2(\alpha)},$$
$$= \frac{2}{\hbar}\frac{\mu^{\rm abxx}(\omega)\cos^2(\alpha) + \mu^{\rm abyy}(\omega)\sin^2(\alpha) + \mu^{\rm abxy}(\omega)\sin(2\alpha)}{\xi^{\rm xx}(\omega)\cos^2(\alpha) + \xi^{\rm yy}(\omega)\sin^2(\alpha)}. \quad (3)$$ eq:vab

For an angle $\alpha = \frac{\pi}{4}$ this expression can be reduced to

$$\mathcal{V}^{\rm ab}(\omega) = \frac{2}{\hbar}\frac{\mu^{\rm abxx}(\omega) + \mu^{\rm abyy}(\omega) + 2\mu^{\rm abxy}(\omega)}{\xi^{\rm xx}(\omega) + \xi^{\rm yy}(\omega)}. \quad (4)$$ eq:vab-90deg

B. Fixing spin

sec:theory-fixspin

Considering that we have 2D structures we can fix the spin direction along the x, y, and z Cartesian coordinates and then define the magnitude of the spin velocity $|\mathcal{V}_{\sigma^{\rm b}}|$ in a fixed angle γ_b as

$$|\mathcal{V}_{\sigma^{\rm b}}|(\omega) = \sqrt{(\mathcal{V}^{\rm ax}(\omega))^2 + (\mathcal{V}^{\rm ay}(\omega))^2}, \quad (5)$$ eq:vs-mag

$$\gamma_{\rm b}(\omega) = \tan^{-1}\left(\frac{\mathcal{V}^{\rm ay}(\omega)}{\mathcal{V}^{\rm ax}(\omega)}\right), \quad (6)$$ eq:gamma-ang

where the angle is measured in the counterclockwise direction from the positive x axis.

C. Fixing velocity.

sec:theory-fixvel

In a similar way we can fix the velocity in the xy plane along x and y directions and define $|\mathcal{V}^{\rm a}|$ as

$$|\mathcal{V}^{\rm a}|(\omega) = \sqrt{(\mathcal{V}^{\rm ax}(\omega))^2 + (\mathcal{V}^{\rm ay}(\omega))^2 + (\mathcal{V}^{\rm az}(\omega))^2}. \quad (7)$$ eq:vv-mag

and the corresponding polar and azimuthal angles θ and φ as

$$\theta(\omega) = \cos^{-1}\left(\frac{\mathcal{V}^{\rm az}(\omega)}{|\mathcal{V}^{\rm a}(\omega)|}\right), \quad 0 \leq \theta \leq \pi, \quad (8)$$ eq:polar-ang

$$\varphi(\omega) = \tan^{-1}\left(\frac{\mathcal{V}^{\rm ay}(\omega)}{\mathcal{V}^{\rm ax}(\omega)}\right), \quad 0 \leq \varphi \leq 2\pi. \quad (9)$$ eq:azimuthal-ang

Layer No.	Atom type	Position [Å] x	y	z
1	H	-0.61516	-1.42140	1.47237
2	C	-0.61516	-1.73300	0.39631
3	C	0.61516	1.73300	0.15807
4	C	0.61516	0.42201	-0.15814
5	C	-0.61516	-0.37396	-0.39632
6	H	-0.61516	-0.68566	-1.47237

TABLE I. Unit cell of *alt* structure. Layer division, atom types and positions for the *alt* structure. The structure unit cell was divided in six layers corresponding each one to atoms in different z positions. The corresponding layer atom position is depicted in Fig. 1 with the corresponding number of layer. tab:alt-unitcell

D. Layer-by-layer analysis.

sec:theory-layer

For a layered system we have that the total contribution of Eqns. (5) and (7) is given[1] by

$$|\mathcal{V}_{\sigma^{\rm b}}(\omega)| = \ell_{\rm eff}\sum_{\ell=1}^{N_{\rm eff}}|\mathcal{V}_{\sigma^{\rm b}}(\ell|\omega)| \quad (10)$$ eq:vs-layer

$$|\mathcal{V}^{\rm a}(\omega)| = \ell_{\rm eff}\sum_{\ell=1}^{N_{\rm eff}}|\mathcal{V}^{\rm a}(\ell|\omega)| \quad (11)$$ eq:vv-layer

III. RESULTS

sec:results

We preset the results for $\mathcal{V}^{\rm ab}$ for the $C_{16}H_8$-alt and $C_{16}H_8$-up structures being both noncentrosymmetric semi-infinite carbon systems with 50% hydrogenation in different arrangements. The *alt* system has alternating hydrogen atoms

Layer No.	Atom type	Position [Å] x	y	z
1	H	-0.61516	-1.77416	0.73196
1	H	0.61518	0.35514	0.73175
2	C	-0.61516	-1.77264	-0.49138
2	C	-0.61516	-0.35600	-0.72316
2	C	0.61516	0.35763	-0.49087

TABLE II. Unit cell of *up* structure. Layer division, atom types and positions for the *up* structure. The structure unit cell was divided in two layers corresponding to hydrogen and carbon atoms.The corresponding layer atom position is depicted in Fig. 2 with the corresponding number of layer. tab:up-unitcell

on the upper and bottom sides of the carbon sheet, while the *up* system has H only on the upper side. We take the hexagonal carbon lattice to be on the xy plane for both structures, and the carbon-hydrogen bonds on the perpendicular xz plane, as depicted in Figs. 1 and 2.

Using the ABINIT code[2] we calculated the self- consistent ground state and the Kohn-Sham states using density functional theory in the local density approximation (DFT-LDA) with a planewave basis. We used Hartwigsen-Goedecker-Hutter (HGH) relativistic separable dual-space Gaussian pseudopotentials[3] including the spin-orbit interaction for calculating $\mathcal{V}^{\rm a}(\omega)$.

The convergence parameters for the calculations of our results corresponding to the *alt* and *up* structures are cutoff energies of 65 Ha and 40 Ha, respectively. The energy eigenvalues and matrix elements were calculated using 14452 **k** points and 8452 **k** points in the irreducible Brillouin zone (IBZ) and present LDA energy band gaps of 0.72 eV and 0.088 eV, respectively for the *alt* and *up* structures. As mentioned in[4], using DFT the LDA is only one method of many other that can be used to calculate the electronic structure of materials. Also it is known that all methods predict a different band gap than the obtained in the experiment. A correction for the band gap energy value can be calculated by other *ab-initio* methods such as the GW approximation[5] being this outside the scope of this paper.

The structures presented here where divided into layers to analyze the he layer-by-layer contribution for $\mathcal{V}^{\rm ab}$ response. The *alt* structure was divided in six layers corresponding the first one to the top hydrogen atoms, from the second to the forth to carbon atoms in different z positions, and the sixth and last one to the bottom hydrogen atoms. The *up* structure was divided into two layers, the first one comprised by the top hydrogen atoms and the second by the carbon atoms. The layer divisions and atom positions for the unit cells are shown in Tables I and II.

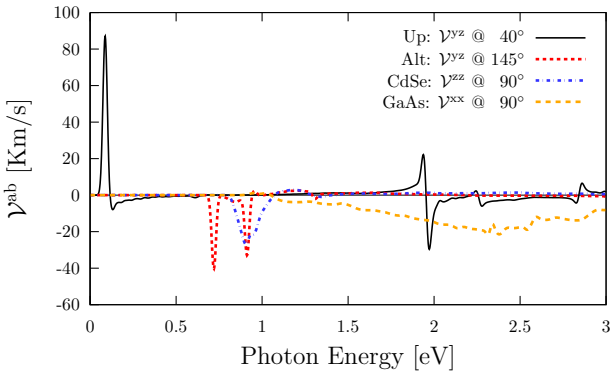

FIG. 3. Comparison of most intense responses for $\mathcal{V}^{\rm ab}$ for *alt*, *up*, CdSe, and GaAs structures. fig:vab-str-comp

A. Spin velocity

sec:res-pure_spin_current_and_spin_velocity

In figure 3

B. Fixing spin

sec:res-fixspin

Lorem ipsum dolor sit amet, consectetuer adipiscing elit. Etiam lobortis facilisis sem. Nullam nec mi et neque pharetra sollicitudin. Praesent imperdiet mi nec ante. Donec ullamcorper, felis non sodales commodo, lectus velit ultrices augue, a dignissim nibh lectus placerat pede. Vivamus nunc nunc, molestie ut, ultricies vel, semper in, velit. Ut porttitor. Praesent in sapien. Lorem ipsum dolor sit amet, consectetuer adipiscing elit. Duis fringilla tristique neque. Sed interdum libero ut metus. Pellentesque placerat. Nam rutrum augue a leo. Morbi sed elit sit amet ante lobortis sollicitudin. Praesent blandit blandit mauris. Praesent lectus tellus, aliquet aliquam, luctus a, egestas a, turpis. Mauris lacinia

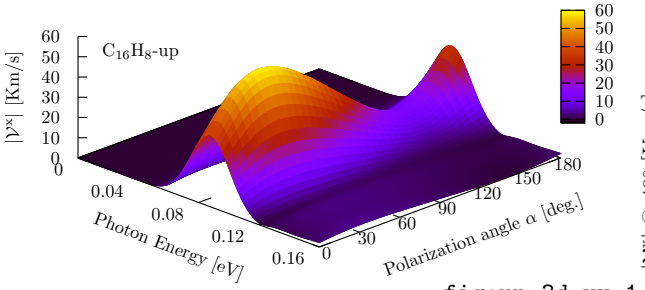

(a) $|\mathcal{V}^{x}|$ for *up* structure fig:up-3d-vx-1

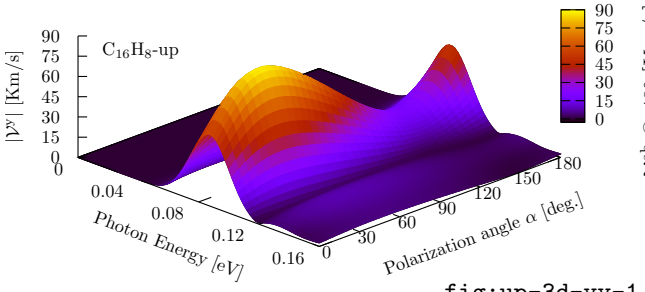

(b) $|\mathcal{V}^{x}|$ for *up* structure fig:up-3d-vy-1

FIG. 4. $|\mathcal{V}^{x}|$ response for $C_{16}H_8$-up structure. The maximum response zone is localized for an energy range from 0.04 eV to 0.12 eV and for a polarization angle of the incoming beam from 25° to 50°. fig:up-3d-1

lorem sit amet ipsum. Nunc quis urna dictum turpis accumsan semper.

C. Fixing velocity

sec:res-fixvel

Up structure.

For the *up* structure we first analyzed the energy range from 0.00 eV to 0.16 eV where we found the most intense response for $\mathcal{V}^{x}$ and $|\mathcal{V}^{y}|$. In Fig. 4 we present the $\mathcal{V}^{a}$ spectra resulting from evaluate again Eq. (7) using different polarization angles α in Eq. (3) but now for the $C_{16}H_8$-up structure. We can see that the onset of the response is when the energy of the incoming light is the same of the gap energy. From this picture we can see that for the zone between the energy range of 0.084 eV-0.093 eV and polarization angles between 30° and 45° is the zone where the maximum zone of response for both, $|\mathcal{V}^{x}|$ and $|\mathcal{V}^{y}|$ is hold. We found that the absolute maximum of the response is obtained when the polarization angle is $\alpha = 40°$ and the energy of the incoming beam is 0.088 eV. In the top frames

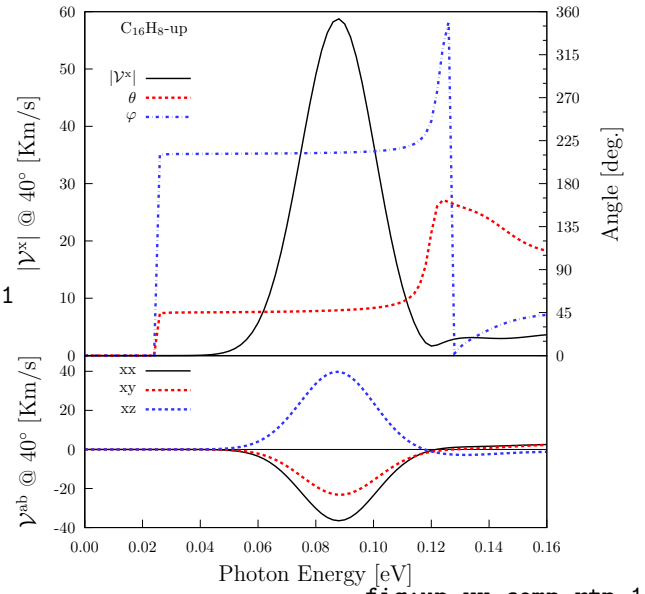

(a) $|\mathcal{V}^{x}|$ fig:up-vx-comp-rtp-1

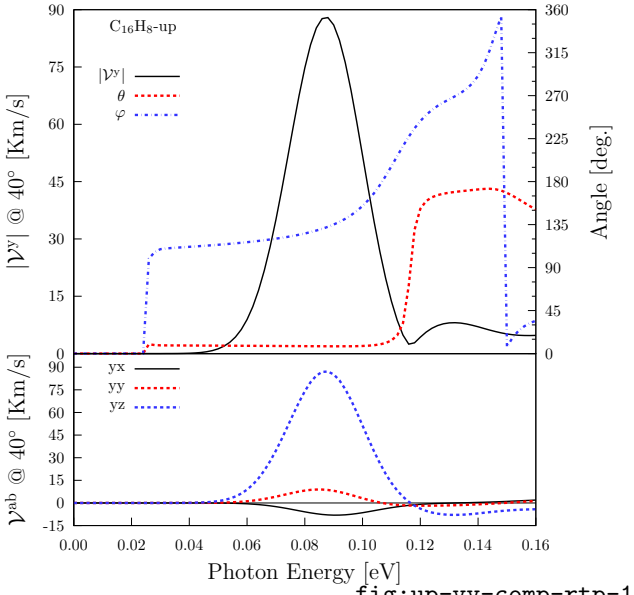

(b) $|\mathcal{V}^{y}|$ fig:up-vy-comp-rtp-1

FIG. 5. Most intense responses of $|\mathcal{V}^{x}|$ and $|\mathcal{V}^{y}|$ and the corresponding three components for the *up* structure. Both maxima where obtained for a polarization angle $\alpha = 40°$. fig:up-vab-comp-rtp-1

of Figs. 5(a) and 5(b) we present the results of $|\mathcal{V}^{x}|$ and $|\mathcal{V}^{y}|$ (left scale) fixing the polarization angle to $\alpha = 40°$ for the *up* structure vs photon energy and the corresponding polar φ and azimuthal θ angles (right scale). In the bottom frames of same figures we present the decomposition of $|\mathcal{V}^{x}|$ and $|\mathcal{V}^{y}|$ in the corresponding $\mathcal{V}^{xx}$,

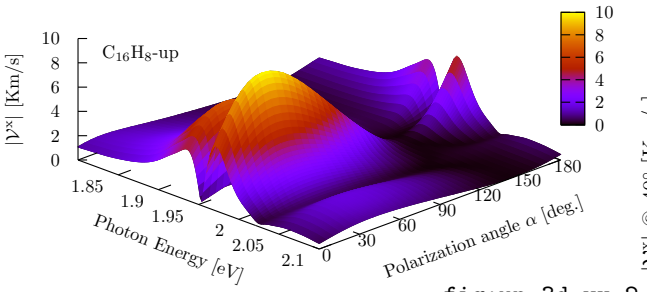

(a) $|\mathcal{V}^{x}|$ for *up* structure fig:up-3d-vx-2

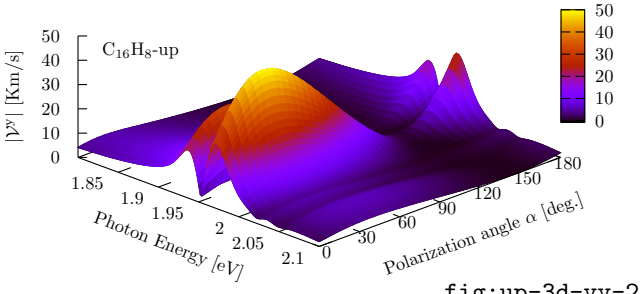

(b) $|\mathcal{V}^{x}|$ for *up* structure fig:up-3d-vy-2

FIG. 6. $|\mathcal{V}^{x}|$ response for $C_{16}H_8$-up structure. The local maximum response zone is localized for an energy range from 1.95 eV to 2.00 eV and for a polarization angle of the incoming beam from 25° to 50°. fig:up-3d-2

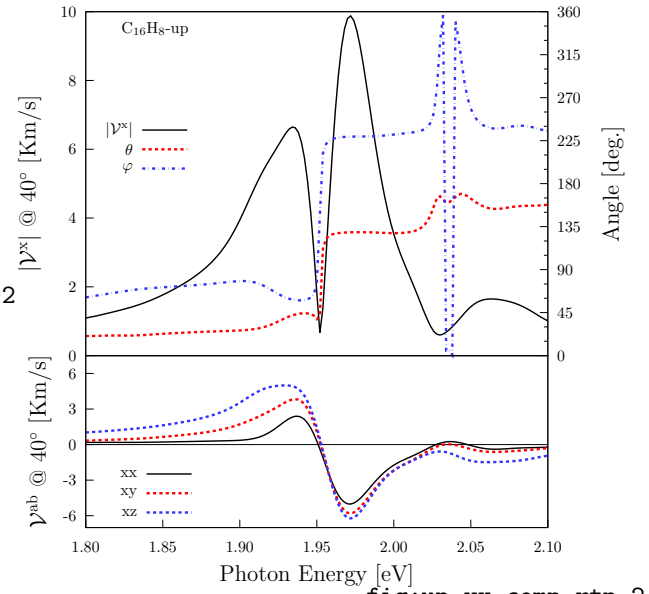

(a) $|\mathcal{V}^{x}|$ fig:up-vx-comp-rtp-2

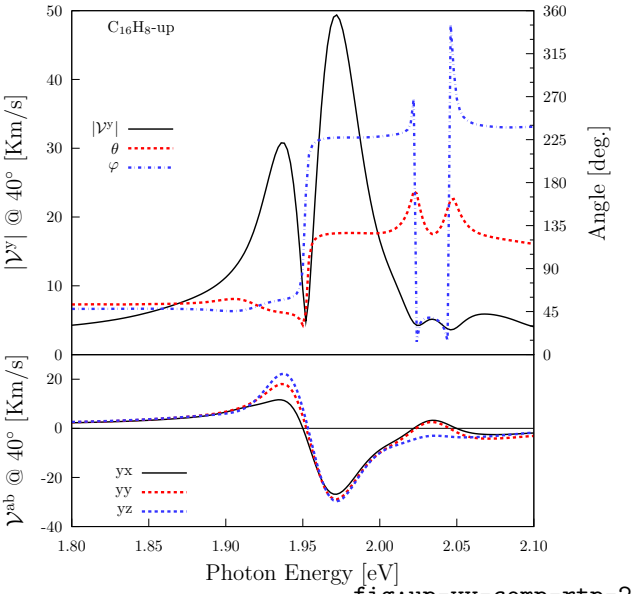

(b) $|\mathcal{V}^{y}|$ fig:up-vy-comp-rtp-2

FIG. 7. Intense responses of $|\mathcal{V}^{x}|$ and $|\mathcal{V}^{y}|$ and the corresponding three components for the *up* structure. Both maxima where obtained for a polarization angle $\alpha = 40°$. fig:up-vab-comp-rtp-2

$\mathcal{V}^{xy}$, $\mathcal{V}^{xz}$, and $\mathcal{V}^{yx}$, $\mathcal{V}^{yy}$, $\mathcal{V}^{yz}$ components with α fixed to 40°.

From Fig. 5(a) we have that for an incoming bean with energy of 0.088 eV the three components have similar contributions and have values of $\mathcal{V}^{xx} = -36.5\,\text{Km/s}$, $\mathcal{V}^{xy} = -23.2\,\text{Km/s}$, and $\mathcal{V}^{xz} = 39.8\,\text{Km/s}$ resulting in a value of $|\mathcal{V}^{x}| = 58.7\,\text{Km/s}$ being this value the absolute maximum obtained when the spin-velocity is fixed in the x direction. To this value corresponds a polar and azimuthal angles of $\varphi = 47.4$ and $\theta = 212.5$, respectively. Now, from Fig. 5(b) we have that the yx and yy components have less contributions for the total response than the yz and for the same incoming beam energy have values of $\mathcal{V}^{yx} = -7.9\,\text{Km/s}$ $\mathcal{V}^{yy} = 8.6\,\text{Km/s}$, and $\mathcal{V}^{yz} = 87.2\,\text{Km/s}$ resulting in a value of the total response of $|\mathcal{V}^{y}| = 87.9\,\text{Km/s}$ being this value the absolute maximum obtained when the spin-velocity is fixed in the y direction and being 1.5 times more intense than $|\mathcal{V}^{x}|$ and corresponding spin polar and azimuthal angles $\varphi = 7.6$ $\theta = 132.7$, respectively. We also found that since the onset of the response till an energy for the incoming beam of 0.118 eV the components of both, $|\mathcal{V}^{x}|$ and $|\mathcal{V}^{y}|$ have no change in the spin polarization direction. Finally, after this energy value both goes to zero. Also there is another energy range of interest for an incoming energy beam from 1.80 eV to 2.10 eV presented in Fig. 6 where two local maxima of $|\mathcal{V}^{x}|$ and $|\mathcal{V}^{y}|$ are obtained for the *up* structure resulting

from evaluate Eqns. (7) and (3). From this figure we have that for the zone between the energy ranges from 1.92 eV to 1.94 eV and from 1.96 eV to 1.98 eV and angles from 30° to 45° those maxima zones are hold. We found that the maxima are obtained when the polarization angle is fixed to 40° and the corresponding energies are 1.934 eV and 1.972 eV. Again, in the top frames of Figs. 7(a) and 7(b) we present the results of $|\mathcal{V}^{x}|$ and $|\mathcal{V}^{y}|$ (left scale) fixing the polarization angle to $\alpha = 40°$ vs the photon energy and the corresponding polar φ and azimuthal θ angles (right scale) for the *up* structure. In the bottom frames of same figures we present the three components xx, xy, xz, and yx, yy, yz corresponding to $|\mathcal{V}^{x}|$ and $|\mathcal{V}^{y}|$ fixing the polarization angle to 40°. We found that for both cases, $|\mathcal{V}^{x}|$ and $|\mathcal{V}^{y}|$, the corresponding components have similar contributions and for an incoming energy beam of 1.934 eV have values of $\mathcal{V}^{xx} = 2.3$ Km/s, $\mathcal{V}^{xy} = 3.8$ Km/s, $\mathcal{V}^{xz} = 4.9$ Km/s, and $\mathcal{V}^{yx} = 11.5$ Km/s, $\mathcal{V}^{yy} = 17.0$ Km/s, $\mathcal{V}^{yz} = 20.4$ Km/s resulting in a in values of $|\mathcal{V}^{x}| = 6.6$ Km/s $|\mathcal{V}^{y}| = 28.7$ Km/s being $|\mathcal{V}^{y}|$ 4.3 times more intense than $|\mathcal{V}^{x}|$ for this photon energy. The responses have polar and azimuthal spin polarization angels $\varphi = 42.0°$ and $\theta = 58.7°$ for $|\mathcal{V}^{x}|$ and $\varphi = 45.2°$ and $\theta = 56.0°$ for $|\mathcal{V}^{y}|$. Alike, for an incoming energy beam of 1.972 eV all the components of $|\mathcal{V}^{x}|$ and $|\mathcal{V}^{y}|$ have similar contributions having values of $\mathcal{V}^{xx} = -5.0$ Km/s, $\mathcal{V}^{xy} = -5.8$ Km/s, $\mathcal{V}^{xz} = -6.2$ Km/s, and $\mathcal{V}^{yx} = -26.8$ Km/s, $\mathcal{V}^{yy} = -28.9$ Km/s, $\mathcal{V}^{yz} = -29.7$ Km/s resulting in a in values of $|\mathcal{V}^{x}| = 9.9$ Km/s $|\mathcal{V}^{y}| = 49.4$ Km/s being $|\mathcal{V}^{y}|$ 5.0 times more intense than $|\mathcal{V}^{x}|$ for this photon energy. The responses have polar and azimuthal spin polarization angles $\varphi = 129.0°$ $\theta = 229.1°$ or $|\mathcal{V}^{x}|$ and $\varphi = 127.0°$ and $\theta = 227.1°$ for $|\mathcal{V}^{y}|$. Finally we have that all the tree components of $|\mathcal{V}^{x}|$ and $|\mathcal{V}^{y}|$ keep the spin polarization positive till an energy of the incoming beam equal to 1.954 eV when the spin polarization changes the direction and after an energy for the incoming beam equal to 2.05 eV both responses goes to zero.

Alt structure.

For the *alt* structure we analyzed the energy range from 0.6 eV to 1.0 eV where we found the most intense response for $|\mathcal{V}^{x}|$ and $|\mathcal{V}^{a}|$. In Fig. 8 we present the $|\mathcal{V}^{a}|$ spectra resulting from evaluate Eq. (7) using different polarization angles α in Eq. (3) for the $C_{16}H_8$-alt structure. We can see that the onset of the response is when the energy of the incoming light is the same of the gap energy. From this picture we can see that for the zone between the energy range of 0.90 eV-0.93 eV and polarization angles between 120° and 150° is the zone where the maximum response for both, $|\mathcal{V}^{x}|$ and $|\mathcal{V}^{y}|$ is kept. We also found that the absolute maximum of the response is obtained when the energy of the incoming bean is 0.912 eV and the polarization angle is $\alpha = 145°$. In the top frames of Figs. 9(a) and 9(b) we present the results for $|\mathcal{V}^{x}|$ and $|\mathcal{V}^{y}|$ (left scale) fixing the polarization angle to 145° for the *alt* structure vs the photon energy and the corresponding polar φ and azimuthal θ angles (right scale). Also in the bottom frames of Figs. 9(a) and 9(b) we present the decomposition of $|\mathcal{V}^{x}|$ and $|\mathcal{V}^{y}|$ in the corresponding components $\mathcal{V}^{xx}$, $\mathcal{V}^{xy}$, $\mathcal{V}^{xz}$ and $\mathcal{V}^{yx}$, $\mathcal{V}^{yy}$ $\mathcal{V}^{yz}$ with α fixed to 145°. Making the analysis for the

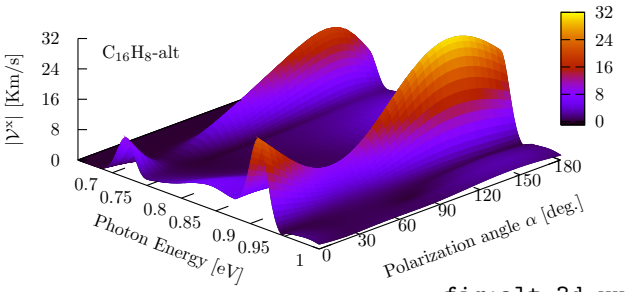

(a) $|\mathcal{V}^{x}|$ for *alt* structure fig:alt-3d-vx

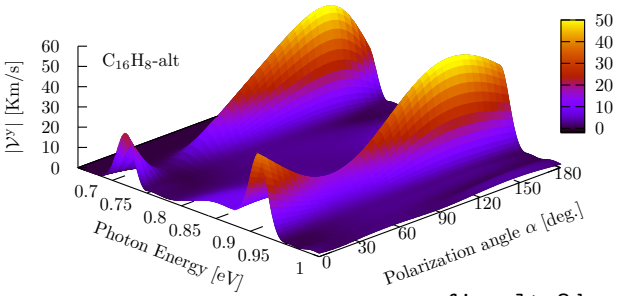

(b) $|\mathcal{V}^{x}|$ for *alt* structure fig:alt-3d-vy

FIG. 8. $|\mathcal{V}^{x}|$ response for $C_{16}H_8$-alt structure. The maximum response zone is localized for an energy range from 0.90 eV to 0.93 eV and for a polarization angle of the incoming beam from 120° to 150°. fig:alt-3d

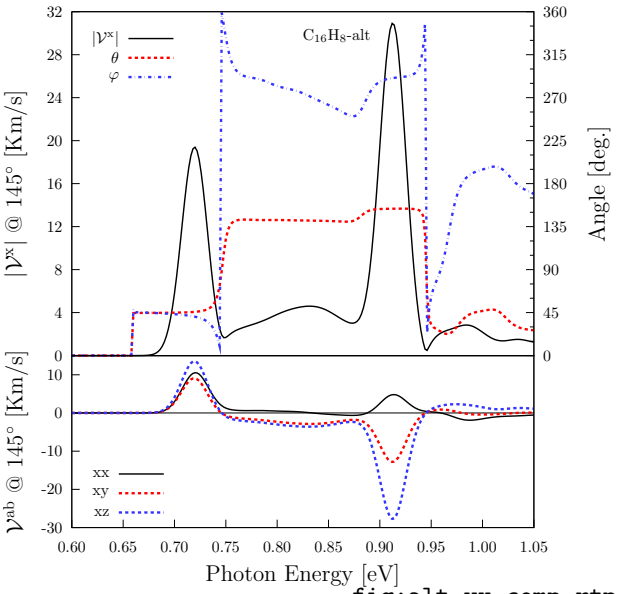

(a) $|\mathcal{V}^{\mathrm{x}}|$ fig:alt-vx-comp-rtp

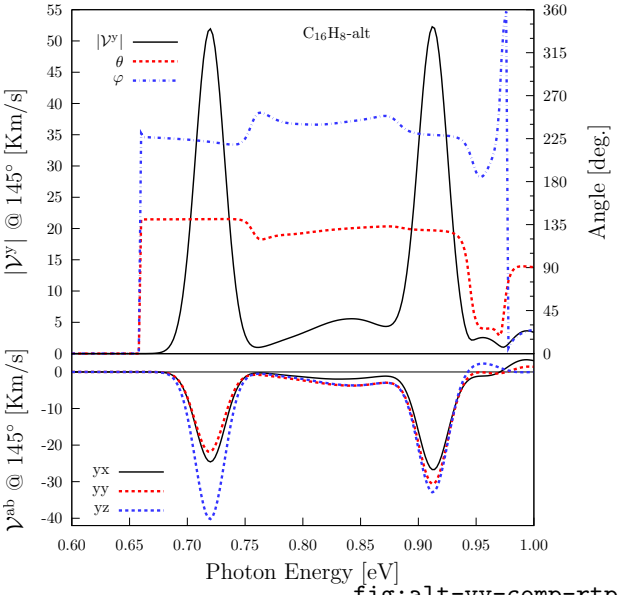

(b) $|\mathcal{V}^{\mathrm{y}}|$ fig:alt-vy-comp-rtp

FIG. 9. Most intense responses of $|\mathcal{V}^{\mathrm{x}}|$ and $|\mathcal{V}^{\mathrm{y}}|$ and the corresponding three components for the *alt* structure. Both maxima where obtained for a polarization angle $\alpha = 145°$. fig:alt-vab-comp-rtp

components and angles for $|\mathcal{V}^{\mathrm{x}}|$ depicted in Fig. 9(a) we can see that for an incoming beam energy of 0.720 eV the components contributions are similar having values of $\mathcal{V}^{\mathrm{xx}} = 10.5\,\mathrm{Km/s}$, $\mathcal{V}^{\mathrm{xy}} = 9.1\,\mathrm{Km/s}$, and $\mathcal{V}^{\mathrm{xz}} = 13.5\,\mathrm{Km/s}$ resulting in a total spin-velocity $|\mathcal{V}^{\mathrm{x}}| = 19.4\,\mathrm{Km/s}$ and spin polar and azimuthal angles $\varphi = 45.8°$ and $\theta = 40.7°$, respectively. In the other hand, for an energy of the incoming beam equal to 0.912 eV we found that the contribution of the components are $\mathcal{V}^{\mathrm{xx}} = 4.8\,\mathrm{Km/s}$ $\mathcal{V}^{\mathrm{xy}} = -12.8\,\mathrm{Km/s}$, and $\mathcal{V}^{\mathrm{xz}} = -27.7\,\mathrm{Km/s}$ having a mayor response coming from the xz component and resulting in a spin- velocity magnitude $|\mathcal{V}^{\mathrm{x}}| = 30.9\,\mathrm{Km/s}$ being this the absolute maximum fixing the spin-velocity in the x direction. Then, the components give us polar and azimuthal angles with values of $\varphi = 153.8°$ and $\theta = 290.4°$. This angles and its variation with the incoming energy beam are presented in the right scale of the top frame of Fig 9(a). Finally we have that since the onset of the response till an energy of the incoming bean of 0.744 eV the three components of $|\mathcal{V}^{\mathrm{x}}|$ are positive while for the range from 0.746 eV to 0.886 eV the $\mathcal{V}^{\mathrm{xx}}$ component is positive but the $\mathcal{V}^{\mathrm{xy}}$ and $\mathcal{V}^{\mathrm{xz}}$ components change in direction. This is due to a change in the spin polarization direction. Finally after the energy value of 0.886 eV the response decreases and goes to zero. Making now the analysis for $|\mathcal{V}^{\mathrm{y}}|$ depicted in Fig. 9(b) we have that for an incoming energy beam of 0.720 eV the yz component have a major contribution than the yx and yy components having values of $\mathcal{V}^{\mathrm{yx}} = -24.6\,\mathrm{Km/s}$, $\mathcal{V}^{\mathrm{yy}} = -21.8\,\mathrm{Km/s}$, and $\mathcal{V}^{\mathrm{yz}} = -40.2\,\mathrm{Km/s}$ resulting in a total spin-velocity $|\mathcal{V}^{\mathrm{y}}| = 51.9\,\mathrm{Km/s}$ and spin polar and azimuthal angles $\varphi = 140.7°$ and $\theta = 221.6°$, respectively. Also, for an energy of the incoming beam of 0.912 eV we found that the contribution of the components are $\mathcal{V}^{\mathrm{xx}} = -26.7\,\mathrm{Km/s}$ $\mathcal{V}^{\mathrm{xy}} = -30.6\,\mathrm{Km/s}$, and $\mathcal{V}^{\mathrm{xz}} = -32.9\,\mathrm{Km/s}$ having all the three components similar contributions and resulting in a spin- velocity magnitude $|\mathcal{V}^{\mathrm{y}}| = 52.3\,\mathrm{Km/s}$ being this the absolute maximum spin-velocity for the velocity fixed to the y direction and being 1.7 times more intense than the maximum of $|\mathcal{V}^{\mathrm{x}}|$. The components then give us the polar and azimuthal angles with values of $\varphi = 129.0°$ and $\theta = 228.9°$, respectively. This angles and the corresponding variation is presented in the right sale of the top frame of Fig. 9(b). We also have that the three components of $|\mathcal{V}^{\mathrm{y}}|$ are negative keeping the same spin polarization since the onset of the response to a energy of the incoming beam of 0.886 eV when the response decreases

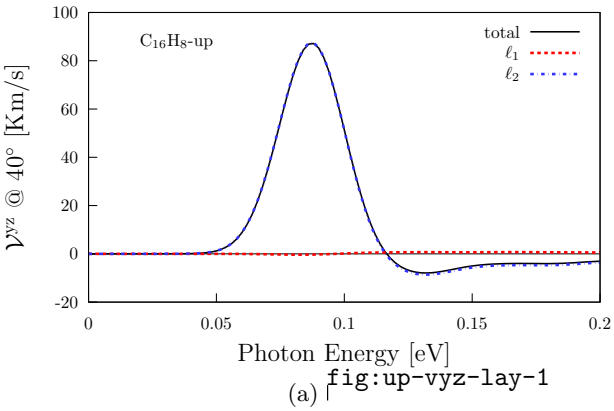

(a) fig:up-vyz-lay-1

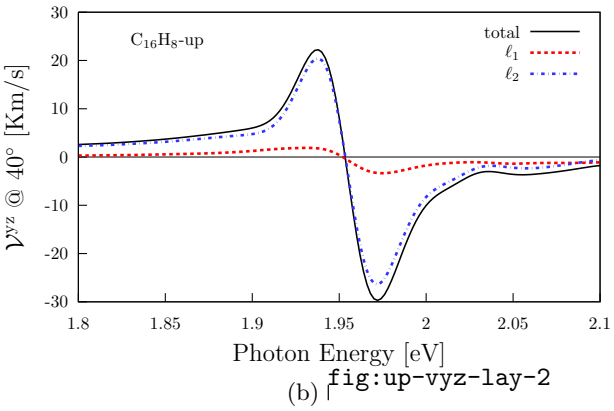

(b) fig:up-vyz-lay-2

FIG. 10. Layer-by-layer contribution of $\mathcal{V}^{yz}$ for the *up* structure. fig:up-vyz-lay

and goes to zero.

IV. LAYER-BY-LAYER ANALYSIS

sec:res-layer_by_layer_analysis

From the bottom frames of Figs. 5 and 7 we can see that for the *up* structure again the most intense component of $|\mathcal{V}^{x}|$ and $|\mathcal{V}^{y}|$ corresponds to $\mathcal{V}^{yz}$ which has a value of 87.2 Km/s for an energy incident beam of 0.088 eV and -29.7 Km/s for an energy incident beam of 1.972 eV. This component and the corresponding layer by layer contribution is depicted in Fig. 10s. From this figure we have that for the energy range from 0 eV to 0.2 eV the response comes from the second layer composed by carbon atoms presented in Tab. II and denoted by the number 2 in Fig. 2. In the other hand, the response for the energy range from 1.8 eV to 2.1 eV almost all the response comes from the carbon atoms having a leaser contribution from the hydrogen layer. From the bottom frames of Fig. 9 we can see that for the *alt* structure the most intense component of $|\mathcal{V}^{x}|$ and $|\mathcal{V}^{y}|$ corresponds to $\mathcal{V}^{yz}$ which has a value of -40.2 Km/s for an energy incident beam of 0.72 eV. This component and the corresponding layer by layer contribution is depicted in Fig. 11. From this figure we have that for the energy range from 0.70 eV to 0.74 eV the fifth and sixth layers corresponding to the bottom carbon and hydrogen numbered with 5 and 6 in Fig. 1 have contributions in opposite direction than the other 4 layers resulting in a total response $\mathcal{V}^{yz} = -40.2$ Km/s for an incoming beam energy of 0.72 eV. In the other hand, for the energy range from 0.88 eV to 0.95 eV the response for the all six layers the responses are in the same direction resulting in a total response $\mathcal{V}^{yz} = -32.89$ Km/s for an incoming beam with energy of 0.912 eV.

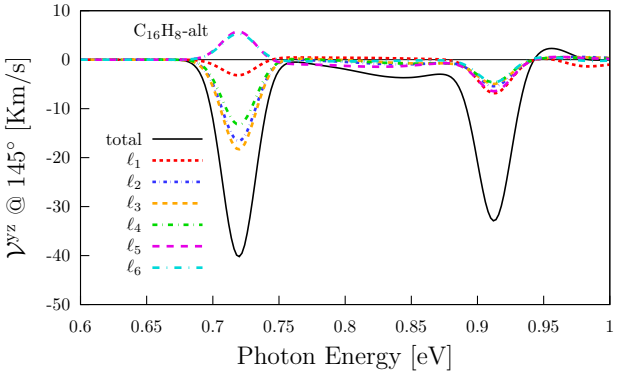

FIG. 11. Layer-by-layer contribution of $\mathcal{V}^{yz}$ for the *alt* structure. fig:alt-vyz-lay

[1] N. Arzate, R. A. Vázquez-Nava, and B. S. Mendoza, Phys. Rev. B **90**, 205310 (2014).

[2] X. Gonze, B. Amadon, P.-M. Anglade, J.-M. Beuken, F. Bottin, P. Boulanger, F. Bruneval, D. Caliste, R. Caracas, M. Côté, T. Deutsch, L. Genovese, P. Ghosez, M. Giantomassi, S. Goedecker, D. Hamann, P. Hermet, F. Jollet, G. Jomard, S. Leroux, M. Mancini, S. Mazevet, M. Oliveira, G. Onida, Y. Pouillon, T. Rangel, G.-M. Rignanese, D. Sangalli, R. Shaltaf, M. Torrent,

M. Verstraete, G. Zerah, and J. Zwanziger, Comput. Phys. Commun. **180**, 2582 (2009).

[3] C. Hartwigsen, S. Goedecker, and J. Hutter, Phys. Rev. B **58**, 3641 (1998).

[4] R. Zapata-Peña, S. M. Anderson, B. S. Mendoza, and A. I. Shkrebtii, physica status solidi (b) **253**, 226 (2016).

[5] G. Onida, L. Reining, and A. Rubio, Rev. Mod. Phys. **74**, 601 (2002).

\LastBibItem